

Frequency domain inversion of strong motions: Application to the 1992 Landers earthquake

F. Cotton and M. Campillo¹

Laboratoire de Géophysique Interne et de Tectonophysique, Université Joseph Fourier
Observatoire de Grenoble, France

Abstract. We present a frequency domain inversion in which the observed earthquake strong ground motions are used to constrain the space-time dependence of slip on a fault. Green's functions are numerically evaluated and the parameters describing the rupture are the local slip, rupture time and rise time. These parameters are simultaneously evaluated without additional constraints. This procedure allows for large variations in the local rupture velocity. The June 28, 1992 Landers earthquake ($M_w = 7.3$) offers an exceptional opportunity to apply this technique to a major strike-slip event. We model the rupture evolution, including local differences in slip durations and variations in rupture velocity. Our final results are in good agreement with other inversion studies, geodetic and surface observations. The main discrepancies occurred at depth and at the end of the Johnson Valley fault. We show that a relatively low resolution could be an explanation for these differences. Rupture velocity and slip are extremely heterogeneous, both along strike and with depth. A moment of 0.90×10^{20} N m was found. The slip distribution shows that this event consists of a series of regions of high slip (subevents) separated by regions of relative low slip. Approximately 50% of the moment was released on the Homestead Valley fault; in this region of large slip, the rupture velocity inferred by our inversion is well constrained and is equal to 3.0 km/s at depth and 2.5 km/s near the surface. Our inversion favors the hypothesis that the duration of the slip at each point of the fault is of the order of the duration of rupture of each subevent.

Introduction

Seismic records in the epicentral region are the most reliable source of information on the history of the development of a rupture and on the time function that describes locally the slip on a fault. The installation of strong motion broad band accelerometers near major faults in several places around the world now makes possible the collection of high-quality data at distances near to the source. Slip distributions on faults have been estimated for several earthquakes using strong ground motion records. Studying the 1979 Imperial Valley earthquake, *Olson and Apsel* [1982] and *Hartzell and Heaton* [1983] used a linear least squares inversion of the local strong motion to obtain the slip that occurred within each of many fault segments during several prescribed time intervals. In those linear inversions, the rupture velocity was allowed to vary only slightly, and the models considered involved a great deal of subjective decision making. To avoid this difficulty, other nonlinear approaches have been proposed which invert for both slip amplitude and rupture time [*Beroza and Spudich*, 1988, *Beroza*, 1991; *Hartzell*, 1989; *Fukuyama and Irikura*, 1986; *Takeo*, 1987; *Steidl et al.*, 1991; *Wald and Heaton*, 1991]. These studies are time domain inversions,

most of which are constrained by requiring that the slip is everywhere positive and by minimizing the differences between adjacent subfaults. *Olson and Anderson* [1988] have investigated the use of a linear frequency domain inversion in which the spatial dependence of the slip function at each frequency is related to the spectral amplitudes of ground motion at that frequency. Each frequency is inverted independently, and the total fault motion is finally obtained by a Fourier transform leading in theory to a complete description of the slip.

This paper proposes a new linearized frequency domain inversion technique. The problem is parametrized using a model in which the fault is represented by subfaults of equal area. We introduce the local slip, rupture time, and rise time as parameters to be directly and simultaneously evaluated without constraints through the inversion of the records. This intentional absence of constraints offers the possibility to study the quality of solution in terms of resolution. We apply this method to the magnitude 7.5 Landers earthquake of June 1992, 28, which was the largest earthquake to strike California in 40 years. Figure 1 shows a map of the rupture breaks together with the location of the epicenter of the Landers earthquake. Discontinuities of the fault trace clearly indicate the complexity of the faulting process. One goal of this paper is to check if the rise time and the rupture velocity can be as heterogeneous as the slip so that strong motion inversions have to take into account the possibility of spatial variation of those two parameters in addition to the slip amplitude.

¹Also at Institut Universitaire de France

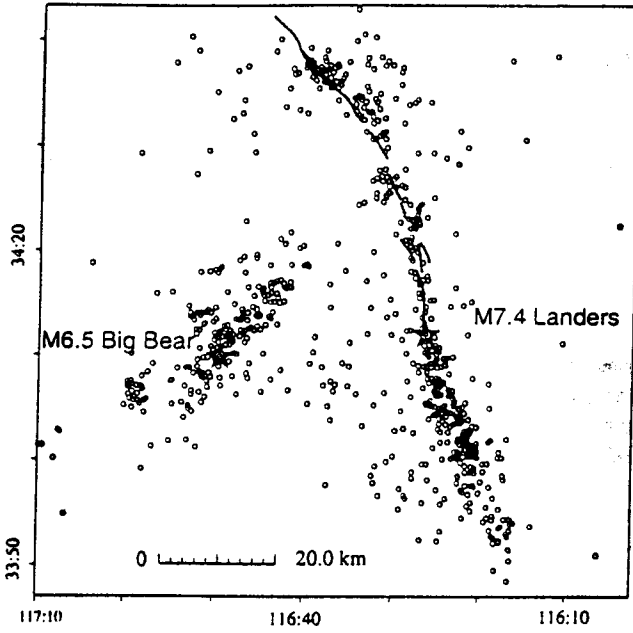


Figure 1. Epicenters of the 1992 M 7.4 Lander and the M 6.5 Big Bear (stars) earthquakes with their aftershocks (circles). Heavy solid lines represent the mapped surface rupture of the Lander earthquake (K. Sieh, California Institute of Technology, written communication, 1992).

Inversion Procedure

Parameterization of Strong Motion Modeling

In this procedure we divide the fault plane into small rectangular regions of equal area called subfaults in the following, and each subfault is allowed to slip once. With this parameterization, the ground motion V at a given station i and a given frequency ω can be represented as a linear sum of n subfault contributions, each appropriately delayed in time to account for front propagation:

$$V_i(\omega) = \sum_{k=1}^n \text{slip}_k \exp[-i\omega t_k] u_{ki}(\omega) S_k[R_k, \omega], \quad (1)$$

where u_{ki} represents the ground motion for a unit constant slip on the subfault k with a given source mechanism, ω is the angular frequency. slip_k , t_k , and S_k are the slip, the rupture time, and the source function of the k th subfault depending on a single variable: the rise time R_k . This simple parametrization allows to limit the number of parameters of the model with respect to the technique proposed by *Olson and Anderson* [1988].

From a practical point of view, each subfault is represented by an array of point sources separated by a distance of less than one sixth of the shortest wavelength. The subfault contributions u_{ki} are obtained by summing the response of these point sources appropriately delayed in time to include the travel time difference due to the propagation of the rupture front across each subfault. A local rupture velocity is therefore assumed for the integration on a subfault and will be discussed later. This local rupture velocity will not be changed in the inversion process. We therefore assumed also that the rupture was unilateral during the earthquake. It is not formally excluded that a series of subfaults break sequentially in a direction opposite to the local rupture propagation on each

subfault. The technique can be refined to avoid this problem in a general case by recomputing the subfault contribution at each step of the inversion. The point source Green functions are calculated for a layered velocity model using the discrete wavenumber integration method [*Bouchon*, 1981] associated with the reflection transmission matrix method [*Kennett*, 1983].

Therefore given a layered crustal model and assuming on each subfault a constant focal mechanism and rupture velocity, $V_i(\omega)$ can be considered as a function of slip, t_k , and R_k if a functional form of the slip function is prescribed (in the following section the influence of this function will be discussed). In this study, the rise time, the slip, and the rupture time on each subfault are inverted simultaneously using the spectral components of the records from several stations in the vicinity of the fault according to the inversion procedure presented in the next section.

Inversion Procedure

The parameter vector p and data vector d are related by the function model vector f as $d=f(p)$. The vector p consists of slip_k , t_k and R_k which appear in equation (1). The elements of d consists of complex three-component spectra from all stations. The f function is a nonlinear function of t_k and R_k . If we assume an initial parameter vector p_0 , we can get the iterative solution p_i by linearization of f around p_0 at the first iteration and around p_{i-1} at each subsequent iteration i . Using the observed data vector d_0 and an inversion algorithm based on the work by *Tarantola and Valette* [1982], p_{i+1} is given by

$$p_{i+1} = p_i + b(A_i^T C_d^{-1} A_i + C_p^{-1})^{-1} [A_i^T C_d^{-1} (f(p_i) - d_0) + C_p^{-1} (p_i - p_0)]. \quad (2)$$

Here A_i is the Jacobian matrix of $f(p_i)$ (the lm th element of A_i is $\delta f_l(p_i)/\delta(p_i)_m$), b is a damping constant between 0 and 1 used to prevent divergence, and C_p and C_d are the covariance matrices for p and d . Because a functional form of the slip is assumed, all derivatives are evaluated analytically. Since this problem is intrinsically nonlinear the final results depend on the starting model chosen a priori.

Quality of the Solution: Analysis of Error and Resolution

The fit to the data at each iteration i is evaluated using the misfit function S [*Tarantola and Valette*, 1982]:

$$S(p_i) = \frac{1}{2} [(f(p_i) - d_0)^T C_d^{-1} (f(p_i) - d_0) + (p_i - p_0)^T C_p^{-1} (p_i - p_0)]. \quad (3)$$

Following *Cohee and Beroza* [1994], we also evaluate the variance reduction between theoretical and observed seismograms defined as

$$\Delta\sigma^2 = 1 - \frac{[d_0 - f(p_{\infty})]^T C_d^{-1} [d_0 - f(p_{\infty})]}{d_0^T C_d^{-1} d_0}. \quad (4)$$

This variance reduction can be computed for all the data but also for each frequency and station component.

The resolution matrix Res illustrates how well the inverse problem can be solved with our data.

$$Res = (A_m^T C_d^{-1} A_m + C_p^{-1})^{-1} A_m^T C_d^{-1} A_m. \quad (5)$$

Table 1. Stations

Station	Network	Abbreviation	Latitude, deg	Longitude, deg	CSMIP Station
Goldstone	Terra	GSC	35.300	-116.804	
Pasadena	Terra	PAS	34.148	-118.172	
Seven Oak Dam	Terra	SVD	34.104	-117.10	
Pinyon Flat Observatory	Terra	PFO	36.169	-121.378	
Amboy	CSMIP	AMB	34.560	-115.74	21081
Barstow	CSMIP	BAR	34.887	-117.047	23559
Baker	CSMIP	BAK	35.272	-116.07	32075
Desert Hot Spring	CSMIP	HOT	33.962	-116.509	12149
Fort Irwing	CSMIP	FOR	35.268	-116.68	24577
Joshua Tree	CSMIP	JOS	34.131	-116.314	22170
Lucerne	Edison	LUC	34.558	116.612	

The farther the resolution operator is from the identity, the worse the resolution is. If the diagonal element of the resolution matrix corresponding to a parameter is equal to 1, the parameter is perfectly resolved by the data set. The trace (sum of the diagonal elements) of Res indicates the number of parameters effectively resolved by the data. The values of the resolution are dependent on the a priori choice of C_p and C_d . For this reason, the resolution matrix in this study is used in a relative way to compare the relative resolution of different parts of the fault or to compare results obtained with different starting models but the same a priori variances.

An Application of This Inversion Procedure to the Landers Earthquake

Data

The strong motion data used in this study come from three sources: 1) accelerograms from the California Division of Mines and Geology network (California Strong Motion Instrumentation Program) which are standard SMA-1 analog recordings [CSMIP, 1992]; 2) force balance accelerometer

digital records from the TERRAScope network [Kanamori *et al.*, 1991]; and 3) an SMA-2 type record from the Southern California Edison Company network in Lucerne Valley.

For each azimuth range, the closest stations were selected. Several stations located in the Los Angeles urban area to the southwest of the epicenter have been removed from the data set. The records given without absolute time were also ignored in the inversion. Table 1 gives the 11 stations used and their locations. The station distribution is shown in Figure 2, which also shows the map view or surface projection of the model fault plane. Each of the 11 stations recorded three components of ground acceleration, and all the components are used in the final inversion.

The accelerograms are band-pass filtered between 20 s and 2.0 s then are doubly integrated in the Fourier domain to obtain particle displacements. The synthetics shown later were filtered in the same way. When the time is available, synthetic and observed waveforms are shown in absolute time. Since there is no absolute time available for Lucerne station, the records are not used in this inversion. Nevertheless, the fit between the synthetics and observed waveshapes at this station is shown.

In the following, 60 frequencies are used. The inversion converges in about 100 iterations (with a damping factor b equal to 0.1). The process is stopped when the decrease of the misfit function is less than 0.2 % from one iteration to the next.

Crustal Model

The model used in this study (Table 2) is the model described in a direct approach of the Landers earthquake rupture done by

Table 2. Crustal Structure Used in Calculation of Green's Function

Depth, km	V_p , km/s	V_s , km/s	Density, Mg/m ³	Q_p	Q_s
0.0	4.1	2.3	2.5	300	300
2.0	5.5	3.2	2.8	500	500
4.0	6.3	3.65	2.9	500	500
26.0	6.8	3.9	3.1	500	500
32.0	8.2	4.7	3.2	500	500

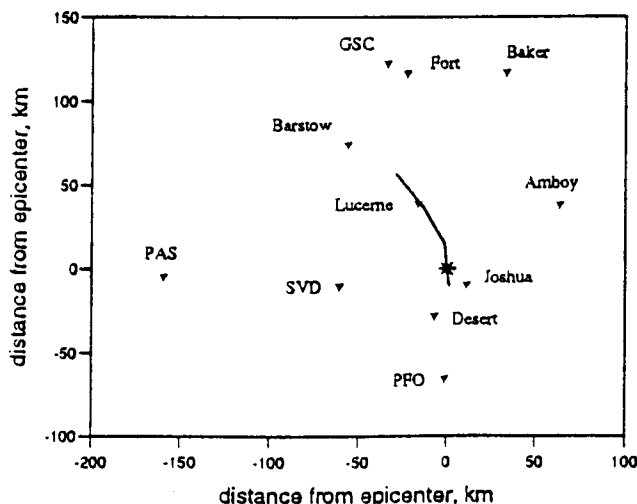


Figure 2. Locations of the stations used in this study. The stations are listed in Table 1. The solid line represents the surface projection of the fault model.

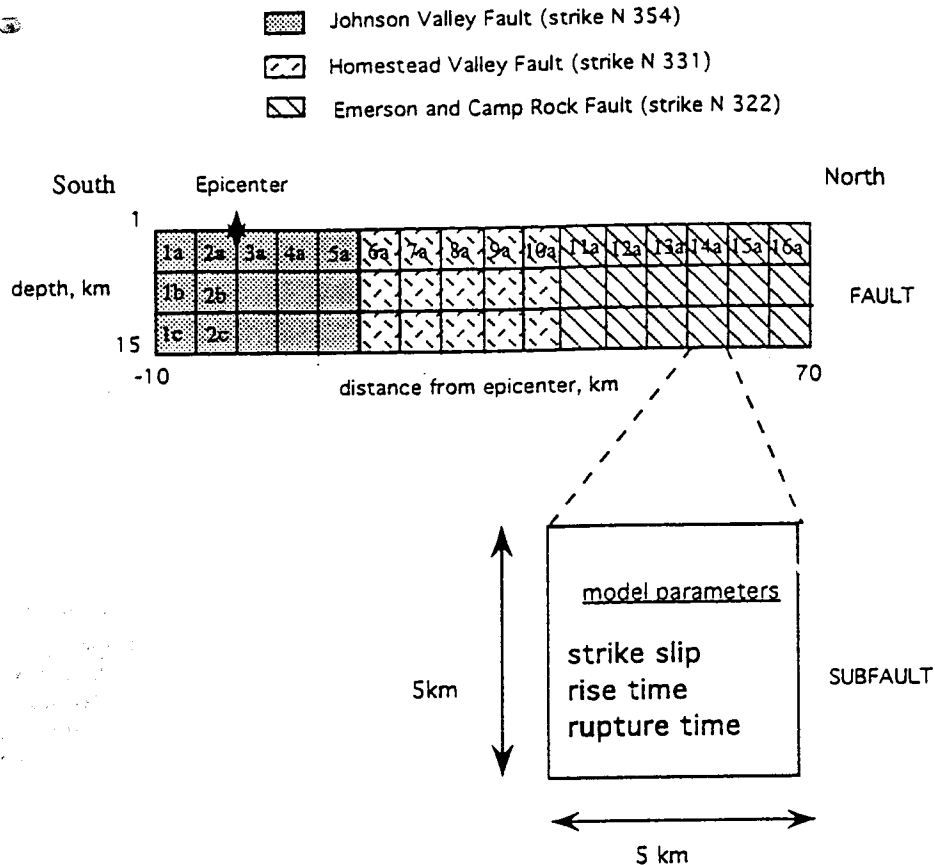


Figure 3. Parameterization of the fault model used in the inversion of strong motion records. The fault is divided in 96 subfaults for which the strike-slip amplitude, rise time, and rupture time are inverted. The epicenter defines the axis origin and is denoted by a star.

Campillo and Archuleta [1993]. This crustal model is adapted from the crustal model for southern California by Kanamori and Hadley [1975] by introducing a surficial low-velocity layer. It consists of four layers over a half-space. Campillo and Archuleta [1993] showed that this lower surficial material is necessary to model the Love waves especially at GSC.

Fault Model

We assume that the surface offset gives an image of the actual fault at depth. The surface breaks show that the Landers rupture involved three different fault segments with different strikes (Figure 1). This observation leads us to consider a model which consists of three distinct segments (30 km, 20 km, and 30 km long, respectively) oriented with different strike azimuths. The three segments represent, from south to northwest, the Johnson Valley, the Homestead Valley, and the Emerson and Camp Rock faults. The fault model extends from a depth of 1 km to 16 km. The fault model is represented in Figure 3. The Landers earthquakes occurred on a series of stepping fault segments, but because of the width of the shear zones (50-200 m according to Johnson *et al.* [1993]) as well as the proximity and the similar strikes of the overlapping segments, it is difficult to resolve the slip on each of the overlapping segments at the periods used here (2 s and greater); we therefore idealize the faults as non overlapping planes. The onset of moment release is delayed by 3 s with respect to the origin time given by the high-frequency first

arrivals to account for a foreshock in the hypocentral region [Campillo and Archuleta, 1993]

Choices

In the starting model, a slip value of 4 m is prescribed on each subfault located between 0 and 60 km north of the epicenter. The others subfaults have no slip. The initial rise time given for each subfault is the same on all the fault plane.

We assume that off-diagonal element of C_d and C_p are equal to 0. The diagonal elements of C_d and C_p are given by the data and parameter variances. As mentioned by Hartzell [1989], the estimation of a priori variances in strong motion inversion is not easy. In our inversion we give a greater weight to the TERRAscope stations which have acquisition system of higher dynamics by giving smaller variances ($C_d=0.25$) to those stations compared to the others ($C_d=1.0$). The final results are comparable to those presented in this paper if the same value of C_d is assumed for all the stations. According to Spudich and Frazer [1984] the slip distribution is strongly dependent on the rupture-front velocity. This effect is clearly shown by Cohee and Beroza [1994] in their inversion of Landers strong motions: the slip distributions found with different rupture front velocities between 2.2 and 3.2 km/s are very different. Since the most important parameter to reproduce is the time at which each point ruptures, we choose to give the rupture time a greater weight in the inversion than either the slip or the rise time of each subfault. We then

Table 3. Moment Estimates and Fit to Data Using Different Parameterizations

Number of Subfaults	Starting Velocity of the Rupture Front, km/s	Initial Rise Time on Each Subfault, s	Slip Function	Mean Resolution, %	Moment, $\times 10^{20}$ N m	Variance Reduction, %
32	3.0	4.0	smooth	68	0.87	65
125	3.0	4.0	smooth	36	0.88	72
48	2.5	4.0	smooth	64	0.89	71
48	3.0	4.0	smooth	65	0.88	70
48	3.0	4.0	rough	68	0.78	63
48	3.0	3.0	smooth	67	0.79	68
48	3.0	2.0	smooth	69	0.68	68
48	3.0	5.0	smooth	63	1.00	57

assume values of smaller a priori variances for the rise time and the slip ($C_p=81.0$) than for the time of rupture of each subfault. ($C_p=169.0$). Like *Fukuyama and Irikura* [1986] and *Fukuyama and Mikumo* [1993] these diagonal values of C_p and C_d were found after several inversion tests to find the best convergence (with a damping constant $b=0.1$).

The observed and synthetic amplitude spectra at each station are equally normalized by the maximum observed amplitude spectra of the three components. This means that for example, the weight given to each station in our inversion is independent of the distance of the station. Indeed, the directivity effect and decay with distance remain present in our proposed physical model.

Tests

Since the inversion is not purely linear, the final results are dependent on the initial parameterization of our model. This dependence leads us to test the influence on our results of some important parameters like the number of subfaults, the shape of the slip function, and the rupture front velocity of our starting model. All those tests have been summarized in Table 3. To compare the quality of the final results obtained with different starting models, the following criteria are used: 1) value of the final misfit, 2) value of the final resolution, and 3)

comparison of the seismic moment obtained from the inversion results with other reliable estimates. The estimates of the moment using long-period data or geological estimates yields values between 0.8 and 1.1 10^{20} N m (Table 4).

To evaluate the influence of the number of subfaults, three different inversions were done with 32, 48, and 125 subfaults, respectively. As the number of subfaults increases, the resolution greatly decreases while the variance reduction remain quite the same (Table 5). Therefore the use of a finer mesh may not resolve the rupture process more accurately. In the following discussion, the model consists on 48 subfaults, each of which has a dimension of 5 km by 5 km. To compute the radiation of each of this subfaults, we used 121 point sources that corresponds to 9 points per shortest wavelength.

The influence of the value of the rise time chosen for all the subfaults in our starting model was evaluated by performing several inversions with a priori values of 2.0, 3.0, 4.0, and 5.0 s (Table 3). The best fits to the data are obtained for rise time of 3.0 and 4.0 s. Since the inversion with an a priori value of 4.0 s leads also to a moment closer to the other independent estimates (Table 4), we choose to consider a value of 4 s in the starting models of the two inversions discussed in the following.

All considerations about the value of the rise time must take into account the specific function used to describe the slip. To test the importance of this factor, we considered two different functions to represent the slip history. They are shown in Figure 4 for a rise time of 4 s. One of the functions is a simple smooth ramp while the other shows a rapid evolution of the beginning of the rupture and a progressive decay of the slope. Although these functions may be regarded as roughly similar, they correspond to quite different slip rates. Therefore they lead to different inversion results, particularly in considering the seismic moment. In the following, we choose to use the function corresponding to a smooth ramp which leads to results that give a better variance reduction and a moment closer to that estimated with long-period data.

Results

We present two models which give similar results in terms of misfit, resolution and moment. The first one was obtained with an initial rupture velocity of 2.5 km/s (model A) and the second one was obtained with an initial rupture velocity of 3.0

Table 4. Moment Estimates

Source	Estimates, $\times 10^{20}$ N m	Method
<i>Sieh et al.</i> [1993]	0.9	geological estimation
<i>Kanamori et al.</i> [1992]	1.1	inversion of teleseismic surface waves
<i>Dziewonski et al.</i> [1993]	1.1	CMT
<i>Murray et al.</i> [1993]	0.8	geodesy (EDM data)
<i>Frey Mueller et al.</i> [1993]	0.9	geodesy (GPS data)

CMT, Centroid Moment Tensor; EDM, Electronic Distance Measurement; GPS, Global Positioning System.

Table 5. Values of the Parameters Obtained for Each Subfault Using an Initial Rupture Velocity of 2.5 km/s (Model A)

	Subfault															
	1a	2a	3a	4a	5a	6a	7a	8a	9a	10a	11a	12a	13a	14a	15a	16a
Rise time, s	2.79	1.77	1.38	2.36	4.03	2.43	2.10	3.34	2.70	2.39	3.18	3.63	2.98	3.33	4.42	3.71
Slip, m	1.29	0.77	0.69	2.07	3.55	1.78	2.44	3.65	3.95	1.20	5.28	4.66	4.48	0.07	1.34	0.49
Time rupture, s	-2.70	-1.16	0.05	1.60	6.77	7.74	9.47	10.65	11.90	13.97	13.56	15.01	20.41	23.15	26.37	24.06

	Subfault															
	1b	2b	3b	4b	5b	6b	7b	8b	9b	10b	11b	12b	13b	14b	15b	16b
Rise time, s	3.06	3.77	4.57	3.20	3.98	1.72	4.12	3.66	3.21	3.17	1.62	3.66	4.13	2.20	3.92	3.76
Slip, m	1.19	0.26	1.40	2.52	2.06	2.32	4.15	3.20	2.85	3.03	2.04	-0.70	4.64	-3.92	-0.60	0.61
Time rupture, s	-5.36	-3.70	-2.65	3.20	4.47	3.82	5.53	7.46	10.46	10.24	16.49	18.05	22.67	20.03	23.83	28.13

	Subfault															
	1c	2c	3c	4c	5c	6c	7c	8c	9c	10c	11c	12c	13c	14c	15c	16c
Rise time, s	3.45	2.16	4.26	3.22	4.46	4.01	4.13	1.44	2.05	1.15	3.88	4.04	4.69	1.48	4.01	3.71
Slip, m	2.73	3.01	2.33	3.03	3.11	2.00	2.07	3.31	2.33	4.65	0.95	5.29	2.52	-3.10	1.11	-1.16
Time rupture, s	-0.43	1.74	0.18	0.40	1.97	9.93	7.99	9.66	10.34	12.81	17.95	22.82	18.01	22.47	26.33	26.45

km/s (model B). The mean variance reduction at each frequency has been calculated with the contribution of all the stations (Figure 5), and this shows that the frequency range over which we fit the data is 0.1-0.3 Hz. Therefore our inversion has a limited spectral resolution, and only the coherent part of the process is taken into account.

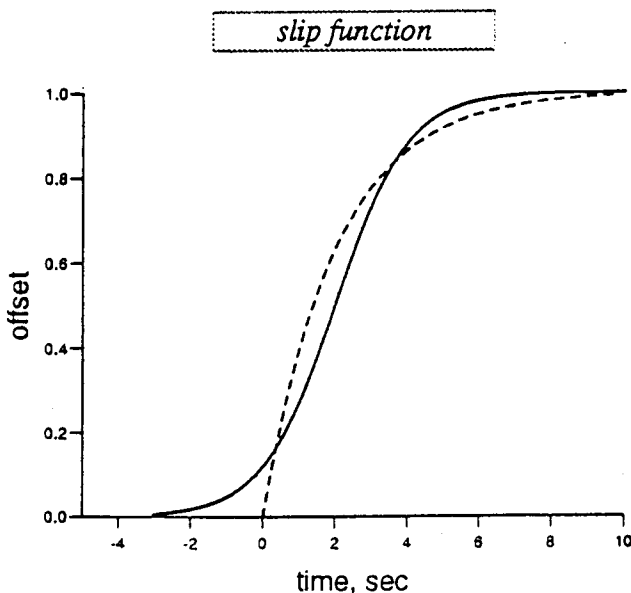


Figure 4. The two slip functions used in this study with a rise time equal to 4 s. For a given rise time R the analytical forms of those functions represented with a solid and a dashed line are respectively $S(t) = 0.5[1 + \tanh((t+R/2.0)(R/2.0))]$ and $S(t) = H(t)(1 - \exp(-2t/R))$, where $H(t)$ is the Heaviside step function.

Table 5 and 6 presents the values of the parameters found for each subfault, while Figure 6a and 7a are smoothed images of the distributions of those parameters. Since our inversion is performed in the frequency domain, the modulus of the synthetic and data spectra of all the station and are shown in Figures 6b and 7b. To present a usual view of the actual fit, the corresponding observed and synthetic time histories are shown in Figure 6c and 7c. The data are the solid lines and the synthetics are plotted as dotted lines at the same scale. For both models, the horizontal components of the TERRAscope stations (PFO, PAS, SVD, and GSC) are very well matched

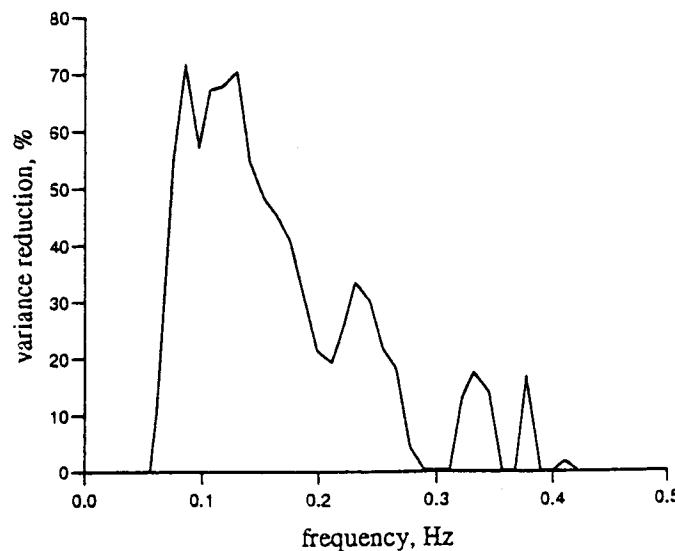


Figure 5. Mean variance reduction computed for each frequency between data of all the stations and synthetics computed with the model described in Table 5.

Table 6. Values of the Parameters Obtained for Each Subfault Using an Initial Rupture Velocity of 3.0 km/s (Model B)

	Subfault															
	1a	2a	3a	4a	5a	6a	7a	8a	9a	10a	11a	12a	13a	14a	15a	16a
Rise time, s	2.81	2.34	1.07	1.51	3.91	1.89	5.62	3.36	2.76	3.93	3.04	3.38	3.31	4.55	3.73	3.87
Slip, m	0.82	0.98	0.53	1.35	-0.04	1.52	2.63	4.27	3.30	1.66	6.07	3.28	-2.89	2.40	-1.22	0.19
Time rupture, s	-2.64	-1.58	-0.03	1.62	3.63	3.70	5.24	10.37	11.92	10.76	13.60	15.25	17.94	20.33	20.32	23.08

	Subfault															
	1b	2b	3b	4b	5b	6b	7b	8b	9b	10b	11b	12b	13b	14b	15b	16b
Rise time, s	3.90	3.98	4.74	3.18	4.50	2.81	2.19	3.53	3.39	4.27	1.78	3.73	2.26	1.53	1.98	4.54
Slip, m	1.76	-0.21	0.82	2.33	3.05	2.53	4.38	4.44	2.63	3.80	2.07	-0.30	1.17	2.44	1.89	1.40
Time rupture, s	-4.23	-2.26	-1.37	3.32	6.64	7.24	9.20	6.16	11.06	9.78	16.20	14.90	16.84	17.50	16.91	24.65

	Subfault															
	1c	2c	3c	4c	5c	6c	7c	8c	9c	10c	11c	12c	13c	14c	15c	16c
Rise time, s	3.06	2.02	4.39	3.31	4.86	4.88	5.15	1.95	3.72	1.26	1.54	3.90	1.56	3.83	0.54	2.66
Slip, m	1.76	-0.21	0.82	2.33	3.05	2.53	4.38	4.44	2.63	3.80	2.07	-0.30	1.17	2.44	1.89	1.40
Time rupture, s	-0.34	1.77	0.12	0.37	1.97	4.04	3.31	9.86	9.51	12.83	12.37	16.86	15.39	18.27	19.81	21.62

both in amplitude and shape. The other horizontal components and even the Lucerne station, which is not considered in our inversion, fit pretty well. Each component is weighted proportionally to the maximum of the spectra of the three components, so the small amplitude vertical components show the smallest variance reduction.

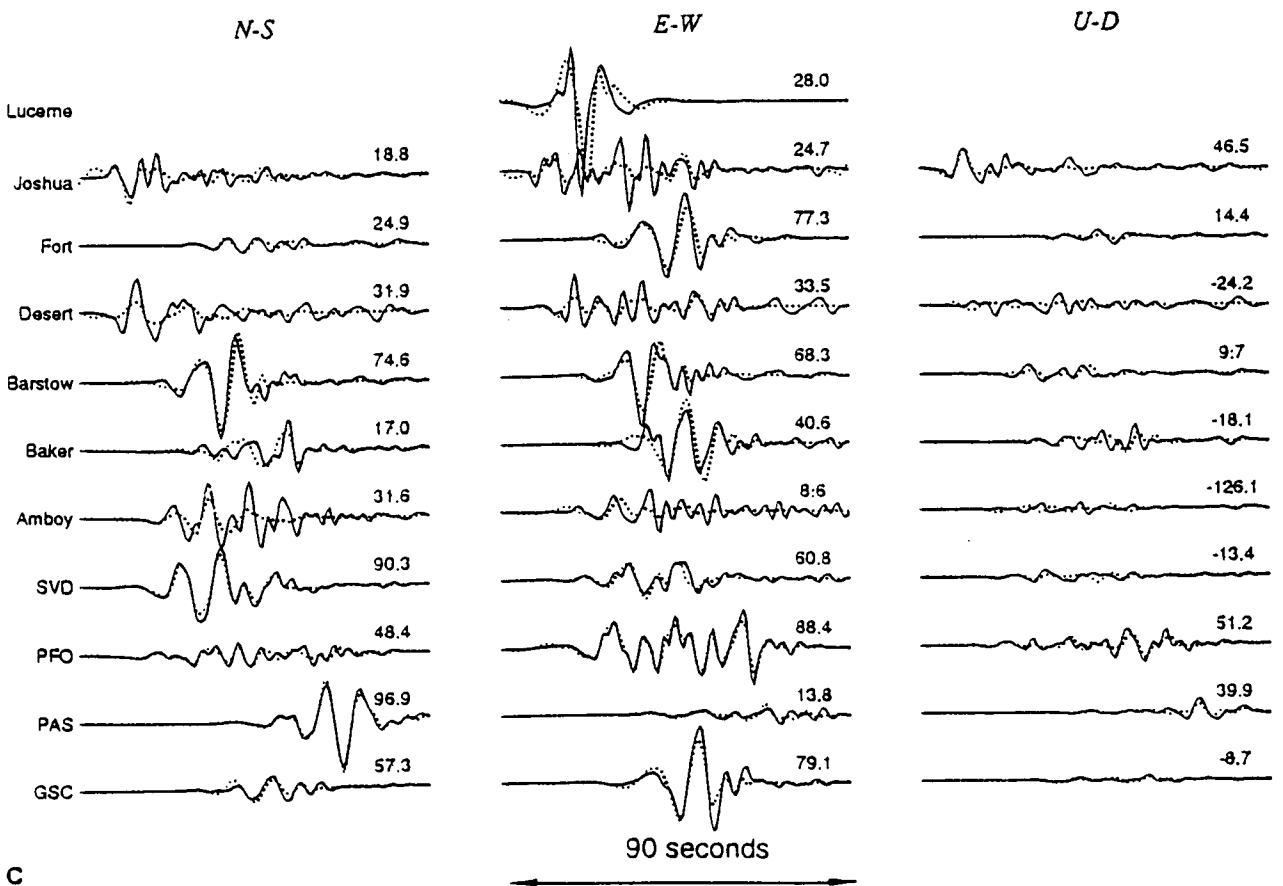
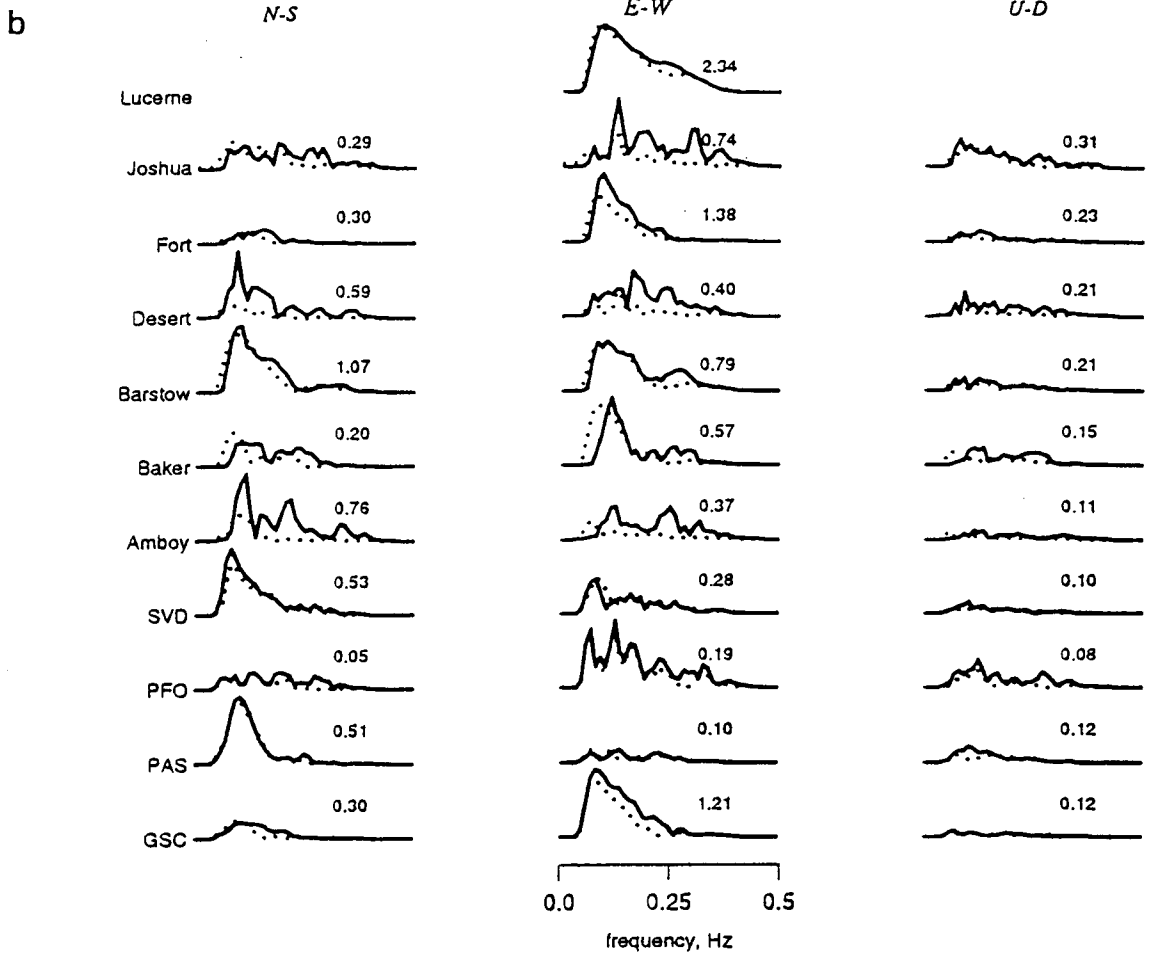
Rupture Evolution

As mentioned above, a strong trade-off is expected between the rupture front velocity and the slip distribution, and our model was allowed to have strong variations of rupture front velocities. In both examples presented, one of the most striking features is that rupture velocity varies strongly with position on the fault. To have a more precise idea of this variation, the times of initial rupture of the subfaults situated at the top, middle, and bottom of the fault are compared for the two final models (Figures 8a, 8b, and 8c). The straight dashed and solid lines represent the time of rupture for a constant rupture front velocity of 3.0 and 2.5 km/s, respectively. For both models, the velocity of the final result significantly differs from the starting value. We find for all the models that a mean value of the rupture front velocity is not representative for the entire length of the fault. The most important characteristic of the two solutions is a common rupture time and rupture velocity where the slip is large (over the first 10 km from the epicenter of the Johnson Valley fault at depth, over the Homestead Valley fault between 25 and 40 km and over the top of the Camp Rock fault between 45 and 50 km near the surface). Along the other regions of the fault, the final value of the rupture velocity and thus the associated slip distribution depend on the a priori rupture velocity. Let us consider only the parts of the fault where the two inversions give the same results. Near the hypocenter the velocity is very

large, specially at depth (more than 3km/s). The rupture front velocity decreases in the second part of the Johnson Valley fault. This relatively fast rupture near the hypocenter is confirmed by *Cohee and Beroza*, [1994]. Their interpretation is that fast rupture could be facilitated by the foreshock generating dynamic stresses that would bring the fault closer to failure just as the mainshock rupture was beginning to propagate northward. According to our inversions, it is difficult to say something about the rupture front velocity between 10 and 25 km from the epicenter. The transition of rupture between the Johnson Valley and the Homestead Valley faults is then poorly constrained. The analysis of rupture evolution along the Homestead Valley fault (between 25 and 45 km) is interesting. The results obtained with our two inversions are convergent, and it is the only part of the fault where we can compare the rupture velocities at depth and near the surface since large slip occurred over the entire depth of the fault. At depth (Figure 8b and 8c), the rupture is faster (3.0 km/s) than near the surface (Figure 8a) where the velocity is only of the order of 2.5 km/s. Such a decrease may be related to the shallow slow velocity layer and seems to confirm the idea that the rupture velocity could be proportional to the shear wave velocity. At the end of the Homestead Valley fault and on the transition with the Emerson/Camprock fault (between 40 and 45 km), we observe a deceleration of the rupture velocity at depth where the rupture ends and an acceleration of up to 3.0 km/s near the surface where the slip remains large (between 45 and 50 km).

Slip Distribution

The total moments of both models (Table 4) fall between 0.8 and 0.9×10^{20} N m which is in good agreement with other



c

Figure 6. (continued)

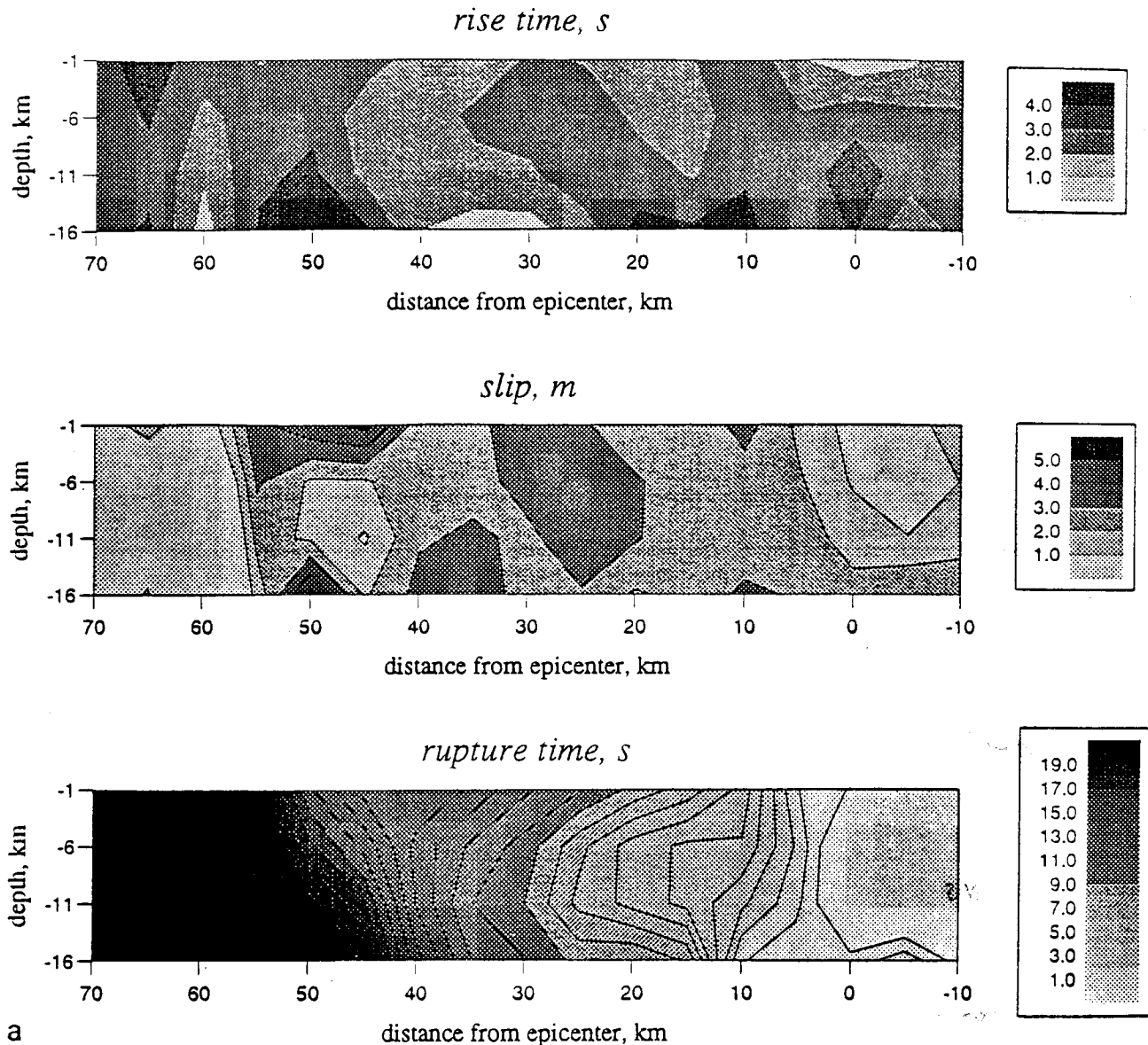
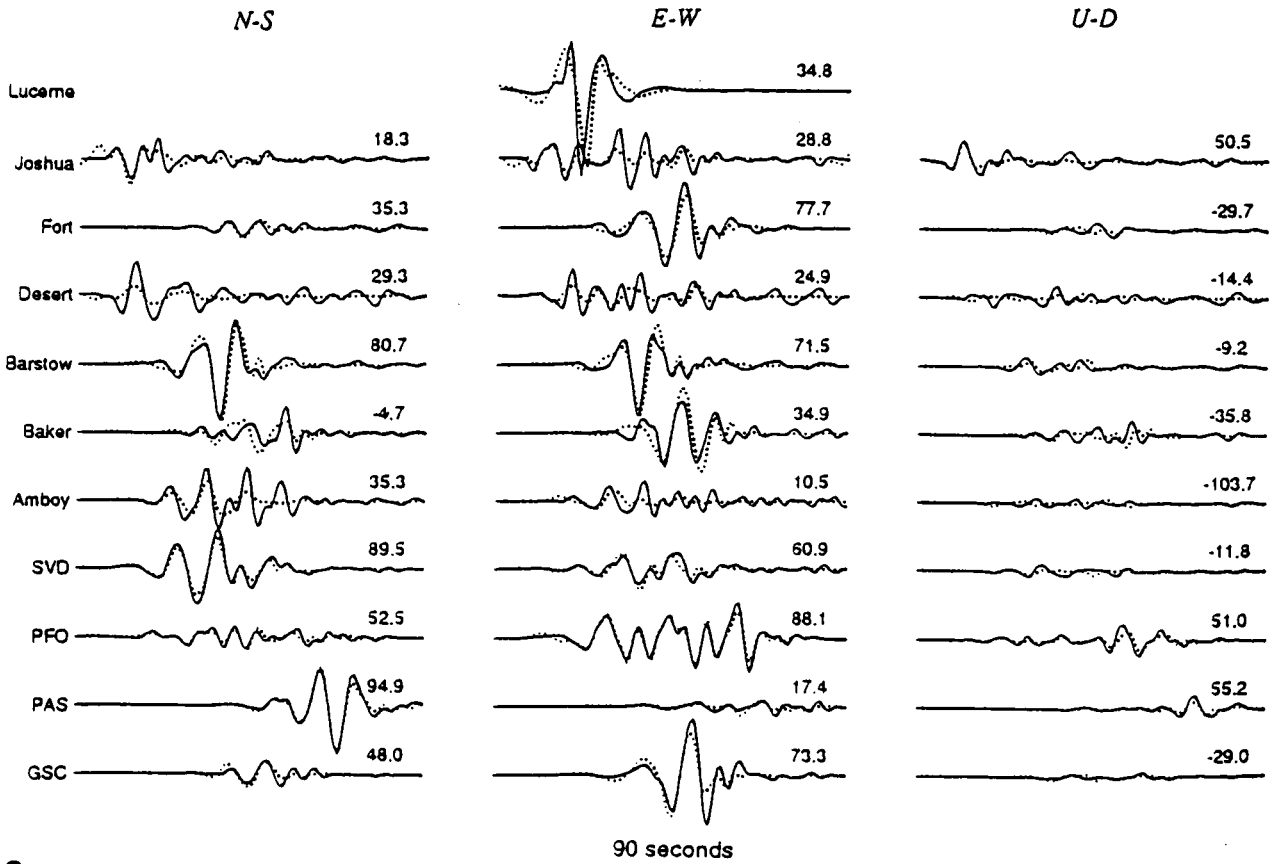
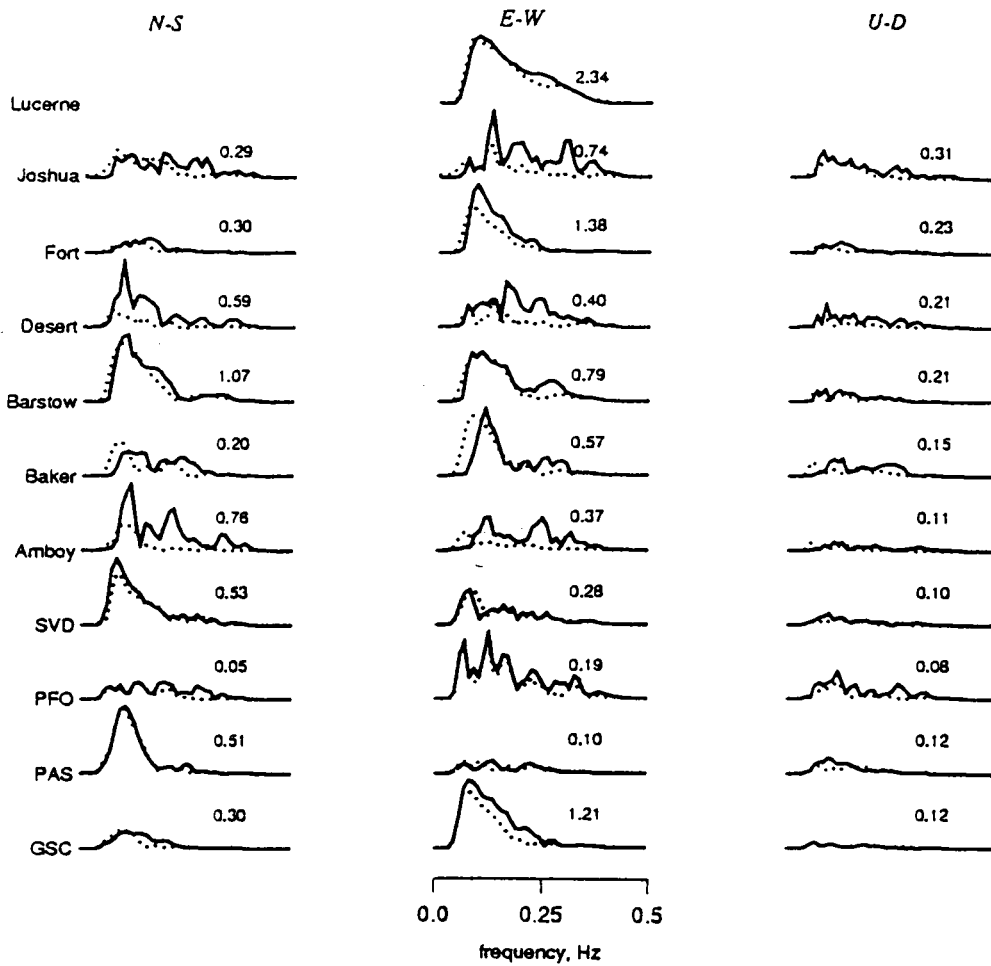


Figure 6. (a) Maps of rupture time, slip, and rise time obtained by interpolation of the results of Table 5 (model A). The 2-s contours are plotted on the map of rupture time to show the evolution of the rupture front. (b) Modulus of the observed spectra (solid line) and synthetic spectra (dotted line) obtained with the fault rupture model described in Table 5 (model A). The maximum in the quantity of mxs of each data amplitude spectrum is shown to the right of each pair. In each case, synthetics and observations are plotted at the same scale. (c) Strong motion seismograms of the Landers earthquake (solid line) compared with synthetic seismograms (dotted line) calculated using the model described in Table 5 (model A). Each pair of data and theoretical seismograms is plotted at the same amplitude scale with the variance reduction shown to the right of each pair.

estimates (Table 3). In both models, significant slip occurred on all three segments. The Johnson Valley fault has about 20% of the total moment, the Homestead Valley fault has 50%, and the Emerson-Camp Rock fault has 30%. Near the hypocenter, in the first part of the Johnson Valley fault, the slip occurred at depth. At the end of the Johnson Valley fault, according to the previous velocity discussion, we believe that the kinematic results are poorly constrained by the strong motion data. Most of the energy radiated by the earthquake comes from the Homestead Valley fault which is situated between 20 and 40 km from the epicenter. The Homestead Valley fault is the only part of the fault where the slip occurred on the entire width of the fault. Slip is important on the Camp

Rock fault, but in this part of the fault, the rupture is shallower. In both map views of the two models presented here, we can see a double peak in the predicted displacement (at about 25 and 45 km) with values of more than 5 m. If we focus our attention on the slip of the subfaults which are at depths of 1-6 km, the maximum slip occurs at a distance between 40 and 45 km from the epicenter. One can notice the presence of negative slip on the edge of the actual rupture zone. In spite of the absence of positivity constraint, the nonphysical negative slip remains small. The absence of positivity constraints allows to perform a resolution analysis that we consider to be important to achieve in strong motion inversions.

b



c

Figure 7. (continued)

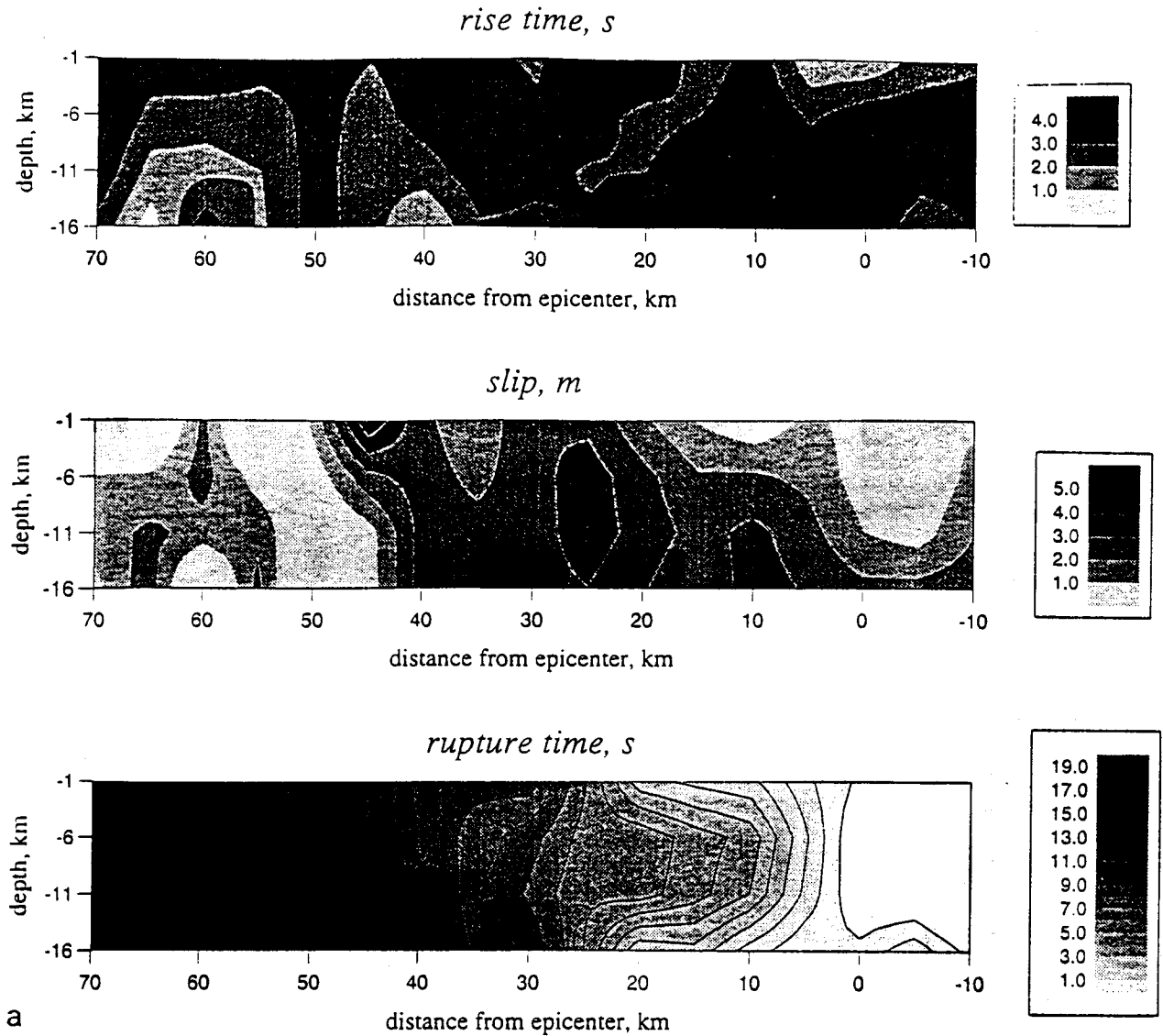


Figure 7. (a) Maps of rupture time, slip, and rise time obtained by interpolation of the results of Table 6 (model B). The 2-s contours are plotted on the map of rupture time to show the evolution of the rupture front. (b) Modulus of the observed spectra (solid line) and synthetic spectra (dotted line) obtained with the fault rupture model described in Table 6 (model B). The maximum in the quantity of m_{xx} of each data amplitude spectrum is shown to the right of each pair. In each case, synthetics and observations are plotted at the same scale. (c) Strong motion seismograms of the Landers earthquake (solid line) compared with synthetic seismograms (dotted line) calculated using the model described in Table 6 (model B). Each pair of data and theoretical seismograms is plotted at the same amplitude scale with the variance reduction shown to the right of each pair.

Rise Time Distribution

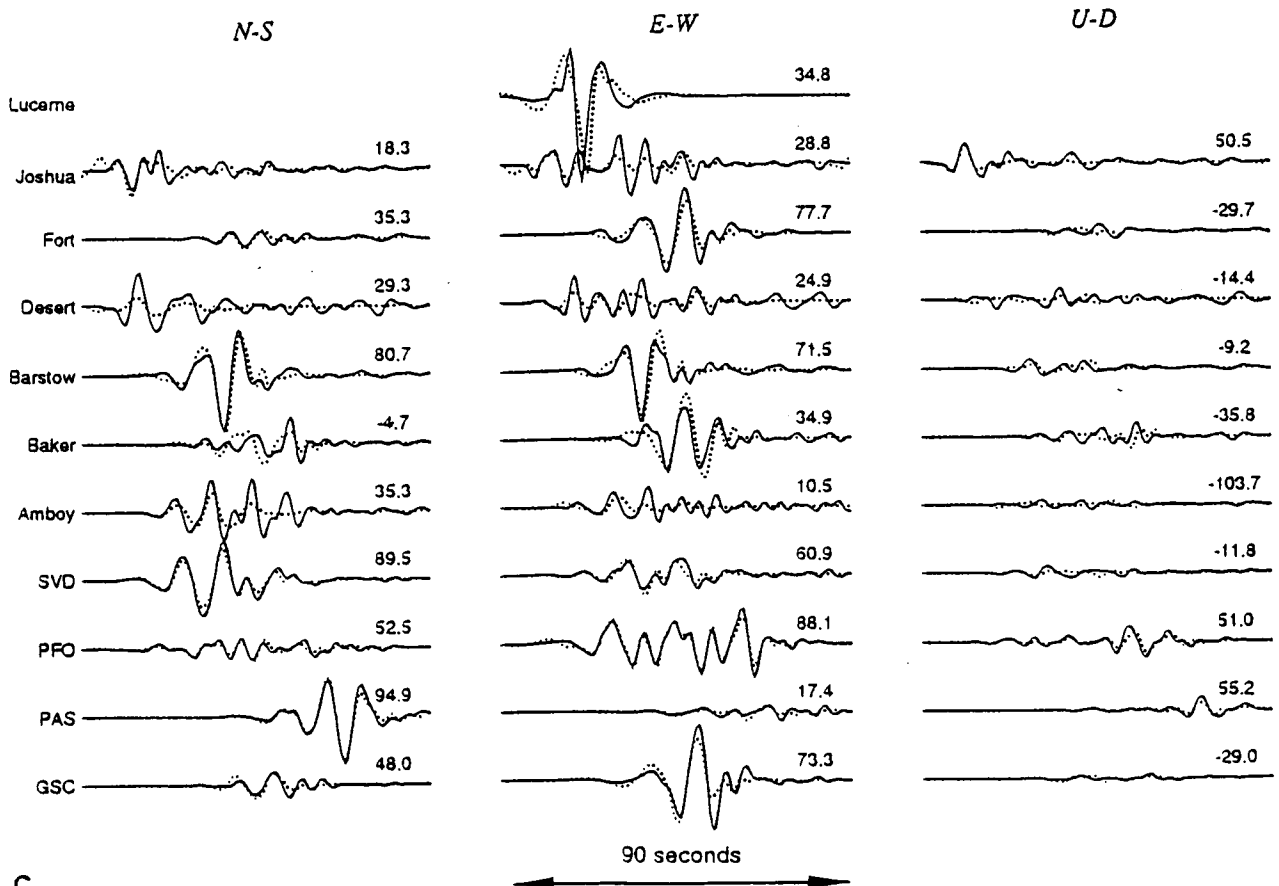
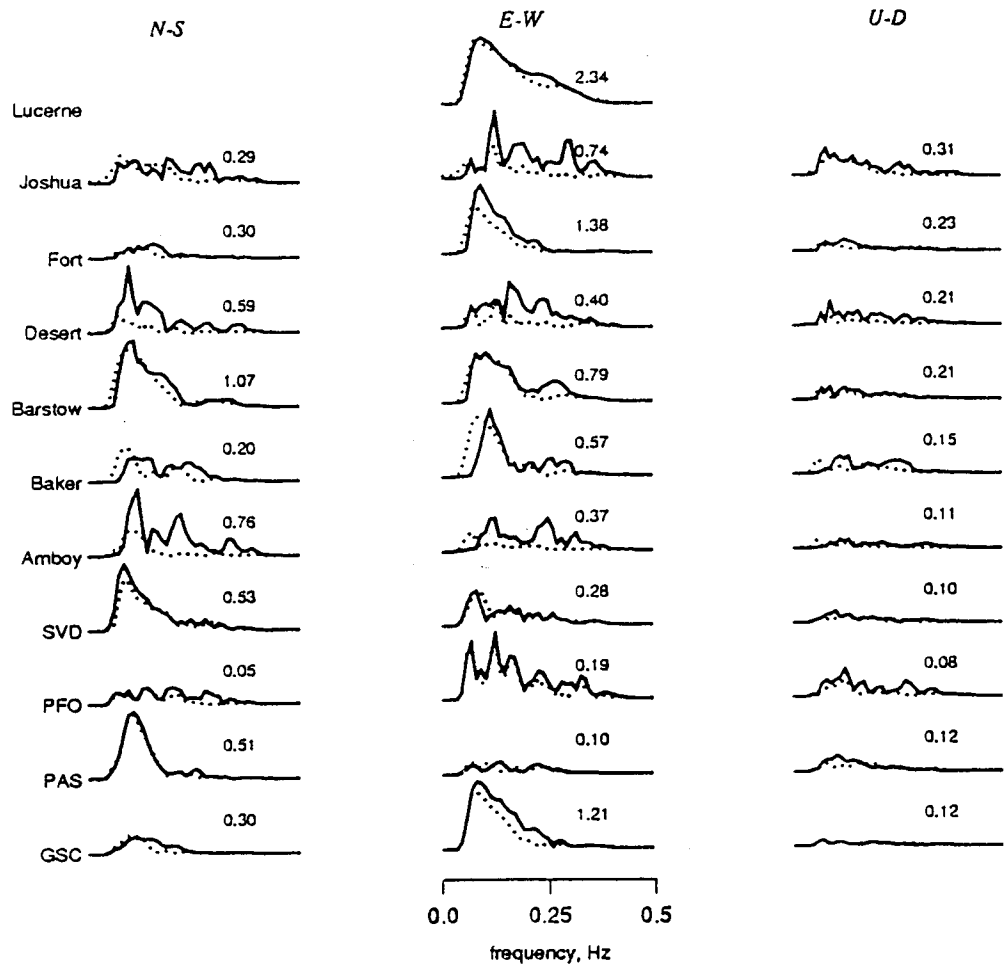
An important feature of our inversion method is that the rise time on each subfault is directly inverted. The rise time distribution is heterogeneous, and if we examine the values of the rise time obtained where the slip is more than 3 m, the final values of the rise time vary from 1.1 s to 5.2 s with most of the values distributed between 3.0 s and 4.0 s. The rise time is larger near the hypocenter and along the Johnson Valley fault than on the Homestead Valley fault and Camp Rock fault. In these regions of high moment release, the mean values of the rise time is between 3.0 and 3.5 s.

We already noticed that values of rise time of about 3-4 s lead to realistic values of the seismic moment. Nevertheless, it is important to check if the inversion of our data alone gives a

Table 7. Final Mean Values of the Rise Time Obtained with Different a Prior Values

Initial Rise Time on Each Subfault, s	Mean Rise Time at the End of the Inversion (Subfaults With Slip > 3.0 m)
1.0	2.74
2.0	2.62
3.0	2.83
4.0	3.37
5.0	4.01

b



c

Figure 7. (continued)

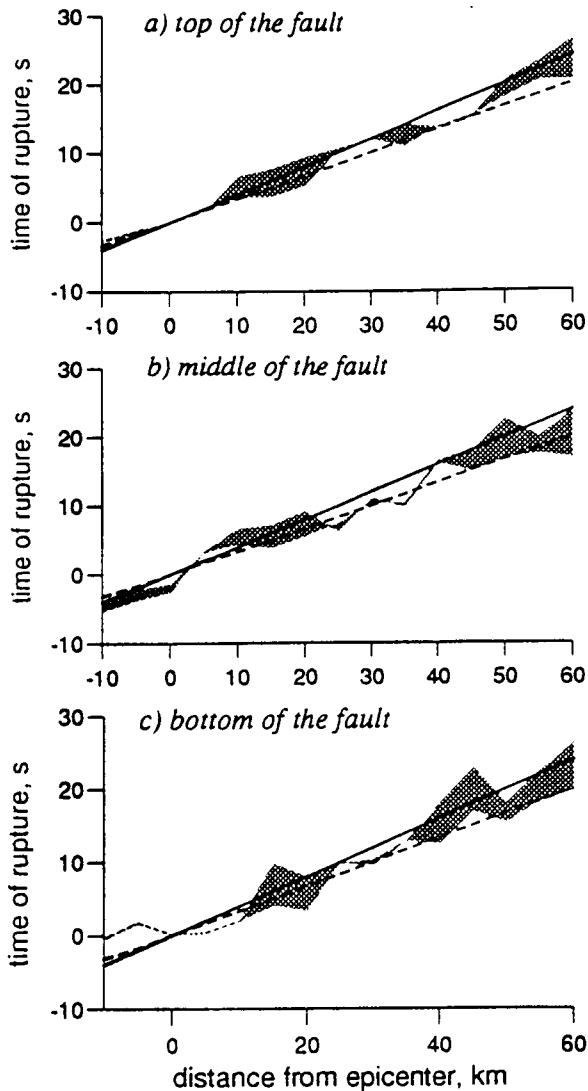


Figure 8. Comparison between the starting values of the time of rupture (straight lines) and the final one obtained by our inversion for both inversions described in the text: the dashed line represents a initial rupture velocity of 3.0 km/s and the solid line represents a starting rupture velocity of 2.5 km/s. The final results of both inversions limit a gray area. Our results are well constrained where this area is thin. (a) Subfaults situated at the top of the fault (depths from 1 to 6 km). (b) Subfaults situated at the middle of the fault (depths from 6 to 11 km). (c) Subfaults situated at the bottom of the fault (depths from 11 to 16 km).

strong constraint on the value of the rise time. We performed a series of inversion with initial values of the rise time between 1 s and 5 s. The results obtained are summarized in Table 7 where the final mean values of the rise time on the zones of high moment release are given. When considering a priori low values as 1 s or 2 s, the inversion converges to larger final values close to 3 s. On the contrary, when considering a priori values of 4 s or 5 s, the inversion tends to decrease the rise time. Indeed, the a priori value of the rise time gives the final value in the regions of low slip where the resolution is weak. This test shows that the value of the rise time is clearly constrained by the data used in this study.

The distance over which rupture is occurring simultaneously is given by the product of rupture velocity by rise time.

According to our results, this distance is at least 9 km (if we consider a mean velocity of at least 3 km/s on the region of high slip release as seen above). The regions of high slip (subevents) have characteristic dimensions between 10 and 20 km which is 50-100% of the typical distance on which the rupture is developing. One can notice that the rise time is larger in the hypocentral area.

Discussions and Conclusions

Resolution of the inversion for the case with an initial velocity of 2.5 km/s is shown in Figure 9. This resolution is computed at the last iteration. The resolution has only small variations from one iteration to another, indicating that the problem is not strongly nonlinear and therefore the iterative linearization is reasonable. This resolution map gives us an idea of the regions of the faults where our inversion is well constrained by the data. The most striking characteristic is that the resolution at depth is less than the resolution at the top of the fault which indicates that the waveforms of strong motions are more dependent on the slip of the subfault situated near the surface than at depth. This result corroborates the study of *Mendoza and Hartzell* [1989], who found that the strong motion records of the September, 19, 1985, Michoacan earthquake recorded at the station Caleta de Campos were relatively insensitive to slip motion across subfaults located at depth. From our imaging, we see that the resolution of the rupture time is relatively poor on the Johnson fault. In this part of the fault, our inversions show a significant difference from the inversions of local records, teleseismic data, or even geodetic data which have been performed using different approaches by *Cohee and Beroza* [1994] or *Wald and Heaton* [1994], and most of the differences between all the proposed model concern the Johnson Valley fault and the adjacent part of the Homestead Valley fault (0 to 25 km from the epicenter). The lack of resolution could be an explanation for those discrepancies. On the other hand, a common characteristic of all the models is a high moment release on the Homestead Valley fault and a shallow rupture on the Camp Rock fault, these are the fault areas where the resolution is high.

Our models show a good agreement with others studies. For example, we found that the fault extends to a greater depth south of the epicenter. The study of guided waves trapped in the fault zone of *Li et al.* [1994] leads to a similar conclusion. According to geological studies [*Sieh et al.*, 1993], the maximum surface slip occurred about 40 km north of the epicenter; our inversion shows similar results near the surface where the maximum slip occurs between 40 and 45 km from the epicenter. Figure 10 shows a complete comparison between the slip of the top subfaults (models A and B) and the mapped surface slip. The agreement can be regarded as a demonstration of the accuracy of our inversion.

The existence of a discontinuity at the fault bend situated at the end of the Johnson fault (20 km from the epicenter) is supported by several seismological results [*Kanamori et al.*, 1992; *Campillo and Archuleta*, 1993; *Li et al.*, 1994] and the surface offsets mapped in the field [*Sieh et al.*, 1993]. The rupture models inferred from strong motions are more complicated than a simple two-sources model but they all show a region of relatively small slip at the end of the Johnson fault [*Cohee and Beroza*, 1994] or at the beginning of the Homestead Valley fault [*Wald and Heaton*, 1994]. Our inversion shows a similar feature with a relatively lower slip

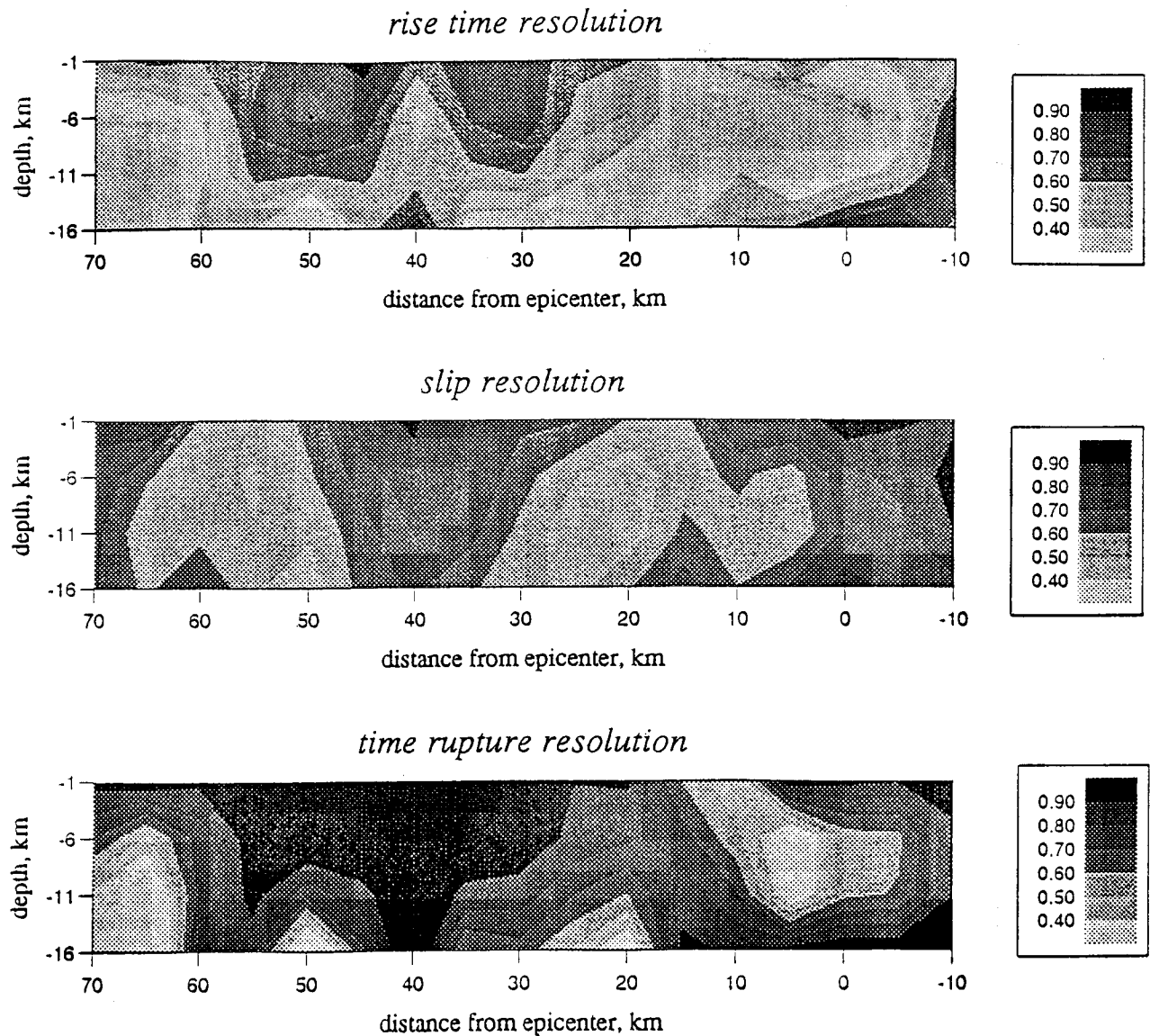


Figure 9. Maps of rise time, slip, and rupture time resolution. These maps are obtained by interpolation of the resolution matrix diagonal value calculated for each inverted parameter. Since those values depends on the choice of the a priori variance of each parameter, these maps are used for relative comparisons of the resolution in different parts of the fault.

at the end of the Johnson Valley fault. Nevertheless the localization of this barrier is not perfectly constrained.

An important goal of strong motion inversion studies is to try to find a causal relation between rupture velocity variations and the slip amplitude distributions. Several studies of previous earthquakes show that the rupture velocity is not constant [Hartzell and Jida, 1990; Zeng et al., 1993] but no simple relation with the slip distribution was found. Cohee and Beroza [1994] suggest that the rupture front slows down as it encounters high-slip regions. According to Wald and Heaton [1994], there is a decrease in the rupture velocity as the rupture propagates through the shallow regions and slows at it nears a fault step over. In this study, we show that the rupture velocity is well constrained only in regions of high moment release (bottom of the beginning of the Johnson Valley fault, Homestead Valley fault, and top of the Camp Rock fault). On the Homestead Valley fault, the velocity is

slower at the top of the fault (2.5 km/s) than at depth (3.0 km/s), and the rupture slows down on the northern Homestead Valley fault before jumping to the top of the Emerson-Camp Rock fault. A similar feature was proposed by Campillo and Archuleta [1993]. This type of behavior for dynamic rupture from one segment to another is predicted by numerical simulation [Harris et al., 1991].

An important result of our inversion concerns the rise time distribution. The time duration of slip at a given point is a key piece of information because it depends on the type of rupture process. Two types of scenarios for the rupture process are proposed. The dislocation-type process was originally proposed by Aki [1968] for kinematic model. With this type of process, recently invoked to describe actual earthquakes by Heaton [1990] and Brune et al. [1990], the duration of the slip is small with respect to the total duration of the rupture process, and there is no large interaction of the different parts

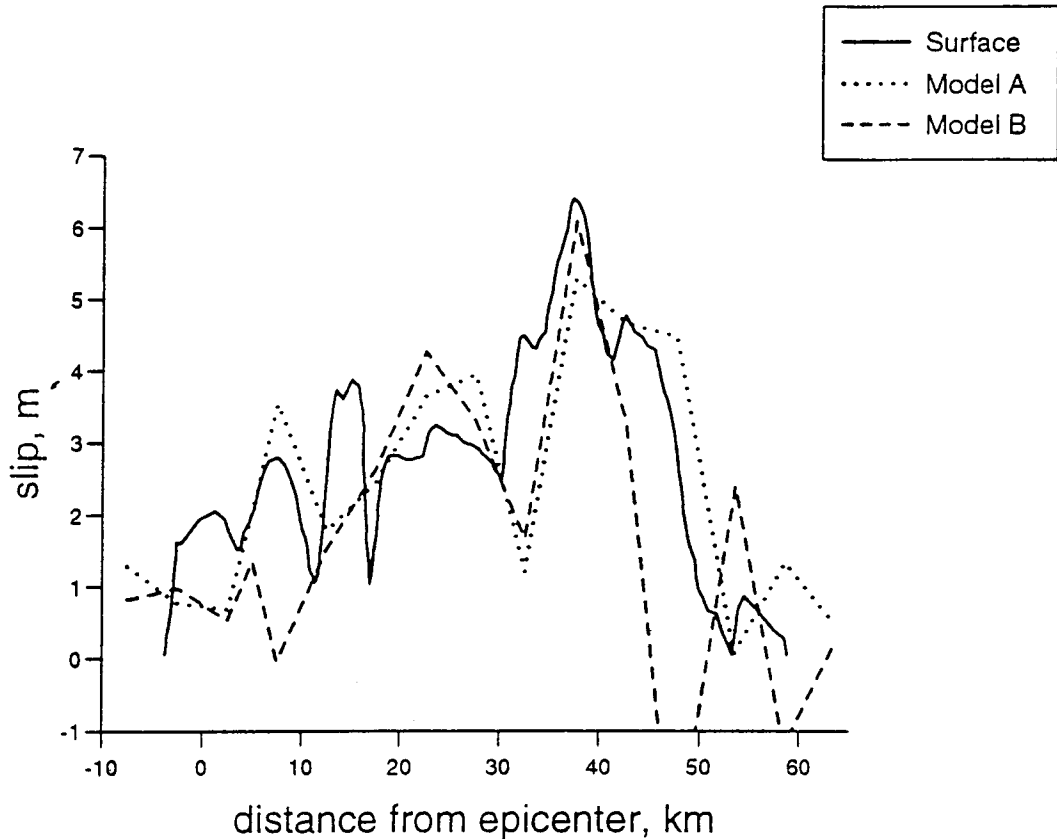


Figure 10. Comparison of fault slip solutions for the subfaults situated at the top of the fault (models A and B) and the mapped surface slip.

of the fault during the dynamic process. On the other hand, in a crack model the slip at each point depends on the slip on the entire fault and consequently the duration of the slip is on the order of the duration of the rupture process [Kostrov, 1964; Madariaga, 1976; Das and Aki, 1977]. According to our results, most of the values of the rise time are between 3.0 and 4.0 s in region where significant slip occurred. The same feature was found by Wald and Heaton [1994], who mention a duration of the order of 4 s in the regions of high slip (near 30-35 km at middepth and for the shallow slip peak at about 40-50 km along strike). The duration of slip is then of the order of the rupture duration of a subevent which have width of about 10 km and is coherent with a crack-type process occurring during each subevent. For such a large earthquake, the slip duration is however smaller than the total rupture duration.

Acknowledgments. We thank R. Archuleta, A. Mendez, and S. Das for their suggestions to improve this work. T. Barr made useful comments on the manuscript. The reviews by G. Beroza, S. Horton, and P. Spudich improved the original manuscript. Thanks are given to CDMG and TERRAscope Network for providing the data.

References

- Aki, K., Seismic displacement near a fault, *J. Geophys. Res.*, **73**, 5358-5376, 1968.
- Beroza, G. C., Near-source modeling of the Loma Prieta earthquake: Evidence for heterogeneous slip and implications for the earthquake hazards, *Bull. Seismol. Soc. Am.*, **81**, 1603-1621, 1991.
- Beroza, G. C., and P. Spudich, Linearized inversion for fault rupture behavior: Application to the 1984 Morgan Hill, California, earthquake, *J. Geophys. Res.*, **93**, 6275-6296, 1988.
- Bouchon, M., A simple method to calculate Green's function for layered media, *Bull. Seismol. Soc. Am.*, **71**, 959-971, 1981.
- Brune, J. N., P. A. Johnson, and C. Slater, Nucleation, predictability and rupture mechanism in foam rubber models of earthquake, *J. Himalayan Geol.*, **1**, 155-166, 1990.
- Campillo, M., and R. J. Archuleta, A rupture model for the 28 June 1992 Landers, California Earthquake, *Geophys. Res. Lett.*, **20**, 647-650, 1993.
- Cohee, B. P., and G. C. Beroza, Slip distribution of the 1992 Landers earthquake and its implications for earthquake source mechanism, *Bull. Seismol. Soc. Am.*, **84**, 692-712, 1994.
- California Strong Motion Instrumentation Program (CSMIP), Processed CSMIP strong-motion records from the Landers, California earthquake of June 1992, report Calif. Dep. of Conserv., Sacramento, 1992.
- Das, S., and K. Aki, A numerical study of two dimensional spontaneous rupture propagation, *Geophys. J. R. Astron. Soc.*, **62**, 591-604, 1977.
- Dziewonski, A. M., G. Ekström, and M. P. Salganik, Centroid-moment tensor solutions for April-June 1992, *Phys. Earth. Planet. Inter.*, **77**, 151-163, 1993.
- Freymueller, J., N. E. King, and P. Segall, The co-Seismic slip distribution of the Landers earthquake, *Bull. Seismol. Soc. Am.*, **84**, 646-659, 1994.
- Fukuyama, E., and K. Irikura, Rupture process of the 1983 Japan Sea earthquake using a waveform inversion method, *Bull. Seismol. Soc. Am.*, **76**, 1623-1640, 1986.
- Fukuyama, E., and T. Mikumo, Dynamic rupture analysis: Inversion for the source process of the 1990, Japan, earthquake, *J. Geophys. Res.*, **98**, 6529-6542, 1993.

- Harris, R. A., R. J. Archuleta, and S. M. Day, Fault steps and the dynamic rupture process: 2-D numerical simulations of a spontaneously propagating shear fracture, *Geophys. Res. Lett.*, **18**, 893-896, 1991.
- Hartzell, S. H., Comparison of seismic waveform results for the rupture history of a finite fault: Application to the 1896 North Palm Springs, California, earthquake, *J. Geophys. Res.*, **94**, 7515-7534, 1989.
- Hartzell, S. H., and T. H. Heaton, Inversion of strong ground motion and teleseismic waveform data for the fault rupture history of the 1979 Imperial Valley, California, earthquake, *Bull. Seismol. Soc. Am.*, **73**, 1553-1583, 1983.
- Hartzell, S. H., and M. Iida, Source complexity of the 1987 Whittier Narrows, California, earthquake from the inversion of strong motion records, *J. Geophys. Res.*, **95**, 12,475-12,485, 1990.
- Heaton, T. H., Evidence for and implication of self-healing pulses of slip in earthquakes rupture, *Phys. Earth Planet. Inter.*, **64**, 1-20, 1990.
- Johnson, A. M., R. W. Fleming, and K. M. Cruikshank, Shear zones formed along long, straight traces of fault zones during the 28 June 1992 Landers, California, earthquake, *Bull. Seismol. Soc. Am.*, **84**, 499-510, 1993.
- Kanamori, H., and D. Hadley, Crustal structure and temporal velocity change in southern California, *Pure Appl. Geophys.*, **113**, 257-280, 1975.
- Kanamori, H., E. Hauksson, and T. H. Heaton, TERRAscope and CUBE project at Caltech, *Eos Trans. AGU*, **72**, 564, 1991.
- Kanamori, H., H. Thio, D. Dreger, E. Hauksson, and T. H. Heaton, Initial investigation of the Landers California earthquake of 28 June 1992 using Terrascope, *Geophys. Res. Lett.*, **19**, 2267-2270, 1992.
- Kennett, B. L. N., *Seismic Wave Propagation in Stratified Media*, Cambridge University Press, New York, 1983.
- Kostrov, B. V., Unsteady propagation of longitudinal shear cracks, *Appl. Math. Mech.*, **28**, 1241-1248, 1964.
- Li, Y. G., K. Aki, D. Adams, A. Hasemi, and W. Lee, Seismic guided waves trapped in the fault zone of the Landers, California, earthquake of 1992, *J. Geophys. Res.*, **99**, 11,705-11,722, 1994.
- Madariaga, R., Dynamics of an expanding circular fault, *Bull. Seismol. Soc. Am.*, **66**, 636-666, 1976.
- Mendoza, C., and S. H. Hartzell, Slip distribution of the 19 September 1985 Michoacan Mexico earthquake: Near source and teleseismic constraints, *Bull. Seismol. Soc. Am.*, **73**, 655-669, 1989.
- Murray, M. H., J. C. Savage, M. Lisowski, and W. K. Gross, Coseismic displacements: 1992 Landers, California, earthquake, *Geophys. Res. Lett.*, **20**, 623-626, 1992.
- Olson, A. H., and J. G. Anderson, Implications of frequency-domain inversion of earthquake ground motion for resolving the space-time dependence of slip on an extended fault, *Geophys. J.*, **94**, 443-455, 1988.
- Olson, A. H., and R. J. Apsel, Finite fault and inverse theory with applications to the 1979 Imperial Valley earthquake, *Bull. Seismol. Soc. Am.*, **72**, 1969-2001, 1982.
- Sieh, K. et al., Near-field investigation of the Landers earthquake sequence, April to July 1992, *Science*, **260**, 171-176, 1993.
- Spudich, P., and L. N. Frazer, Use of ray theory to calculate high-frequency radiation from earthquake sources having spatially variable rupture velocity and stress drop., *Bull. Seismol. Soc. Am.*, **74**, 2061-2082, 1984.
- Steidl, J. H., R. J. Archuleta, and S. H. Hartzell, Rupture history of the 1989 Loma Prieta, California, earthquake, *Bull. Seismol. Soc. Am.*, **81**, 1573-1602, 1991.
- Takeo, M., An inversion method to analyse the rupture processes of earthquakes using near-field seismograms, *Bull. Seismol. Soc. Am.*, **77**, 490-513, 1987.
- Tarantola, A., and B. Valette, Generalized nonlinear inverse problem solved using the least squares criterion, *Rev. Geophys.*, **20**, 219-232, 1982.
- Wald, D. J., and T. H. Heaton, Rupture model of the 1989 Loma Prieta earthquake from the inversion of strong-motion and broadband teleseismic data, *Bull. Seismol. Soc. Am.*, **81**, 1540-1572, 1991.
- Wald, D. J. and T. H. Heaton, Spatial and temporal distributions of slip for the 1992 Landers, California, earthquake, *Bull. Seismol. Soc. Am.*, **3**, 668-691 1994.
- Zeng, Y., K. Aki, and T. Teng, Source inversion of the 1987 Whittier Narrows earthquake, California, using the isochron method, *Bull. Seismol. Soc. Am.*, **83**, 358-377, 1993.

M. Campillo, Laboratoire de Géophysique Interne et Tectonophysique, BP 53 X, Grenoble Cedex, France. (e-mail: campillo@lgit.observ-gr.fr)

F. Cotton, Laboratoire de Géophysique Interne et Tectonophysique, BP 53 X, Grenoble Cedex, France. (e-mail: cotton@lgit.observ-gr.fr)

(Received February 7, 1994; revised August 1, 1994; accepted August 11, 1994.)